Supporting Information for "Stratospheric balloon observations of infrasound waves from the January 15 2022 eruption of the Hunga volcano, Tonga"

Aurélien Podglajen[1], Alexis Le Pichon[2], Raphaël F. Garcia[3], Solène Gérier[3],

Christophe Millet[2], Kristopher Bedka[4], Konstantin Khlopenkov[5], Sergey

Khaykin[6], Albert Hertzog[7]

[1]Laboratoire de Météorologie Dynamique (LMD/IPSL), École polytechnique, Institut polytechnique de Paris, Sorbonne Université, École normale supérieure, PSL Research University, CNRS, Paris, France

[2]CEA, DAM, DIF, 91297 Arpajon, France

[3]Institut Supérieur de l'Aéronautique et de l'Espace (ISAE-SUPAERO), Université de Toulouse, 10 Ave E. Belin 31400 Toulouse, France

[4]NASA Langley Research Center, Hampton, Virginia, USA

[5]Science Systems and Applications, Inc., Hampton, Virginia, USA

[6]Laboratoire Atmosphères, Observations Spatiales (LATMOS), UVSQ, Sorbonne Université, CNRS, IPSL, Guyancourt, France

[7]Laboratoire de Météorologie Dynamique (LMD/IPSL), Sorbonne Universit, École polytechnique, Institut polytechnique de Paris, École normale supérieure, PSL Research University, CNRS, Paris, France

Contents of this file

2. Figures S1 to S2

Introduction

This supplementary information contains a description of the effects of the correction to raw pressure data (Equation (1) of the paper) (S1), a description of the methodology used to derive stereoscopic cloud top height in the HT-HH plume from Himawari-8 and GOES-17 brightness temperature data (S2), details on infrasound travel speed estimations (S3) and a comparison of background pressure variability between balloon STR1 and ground station IS22 (S4).

Text S1.

As mentioned in Sect. 2.1 of the paper, we attempt to correct for the effect of vertical motion of the balloon in the hydrostatic pressure gradient

$$p = p_l \exp\left(\frac{g}{R_d T}\zeta'\right) - \overline{p} \tag{1}$$

where p_l is the raw (balloon-following) pressure and p the Eulerian pressure which would be measured in the absence of altitude variations. Without a high-frequency inertial measurement unit (IMU) onboard, 30-s vertical GPS position has to be interpolated at 1 s to compute ζ'. The raw pressure and Eulerian (corrected) pressure spectra are shown in Fig. S1. The correction effectively cancels out balloon neutral oscillations and affects the spectra up to $\sim$17 mHz (half the sampling frequency of ζ'). It is likely that hydrostatic pressure flucatuations are still impacting data above that frequency, but the temporal resolution of the altitude dataset does not enable us to account for that effect. We anticipate that an IMU would enable to extend the range to both lower and higher frequencies. Fortunately, the power spectral density of altitude fluctuations drops sharply

above the balloon oscillation frequency (e.g., Podglajen et al., 2016), so that the correction becomes unnecessary as its spectrum likely falls below geophysical pressure signals such as the oceanic microbarom, and infrasound from the Hunga eruption or eathquakes.

Besides sampling frequency, another limiting factor is the precision of GPS data, which induces a noise floor in the correction. Our estimates however puts this noise floor either below or at the level of observed background pressure fluctuations, making the correction useful. A last limiting factor which is not well-constrained in our analysis is the lag between pressure and position measurements. We tried to account for this small time shift (a few hundreds of ms), but it may be variable, which would result in an imperfect cancellation of motions around the balloon oscillations (as might be suspected from Fig. S1). Hence, no conclusion can be drawn regarding the actual atmospheric variability near the frequency of balloon oscillation.

Nevertheless, for the purpose of our study, the correction performs well enough (Fig. S1) and is essentially cosmetic, since it does not affect the infrasound range above 20 mHz. Yet, it enables us to more clearly identify the isolated bump related to Hunga infrasound, which otherwise sometimes remains merged with that of the balloon oscillations.

Text S2.

Two primary steps were used in the derivation of cloud top height for the Hunga eruption cloud based on GOES-17 and Himawari-8 geostationary satellite observations: 1) spatially matching simultaneous observations from the two satellites, and 2) using the stereoscopy principle to construct a 3D profile of the cloud. Because the two satellites have sufficiently different viewing angles, then it can be possible to derive a cloud top height with accuracy

equal to or better than the spatial resolution of the imagery being used. Level 1B infrared (IR) brightness temperature (BT) data in the 10.3 μm is collected at 2 km/pixel nadir resolution and nearly simultaneously from GOES-17 and Himawari-8 because the imagers on these satellites, the Advanced Baseline Imager (ABI) and Advanced Himawari Imager (AHI) respectively, are nearly identical and have the same scan initiation times and scan rate. Although IR imagery is of lower resolution than the visible, it has its own advantages as it is free of shadows, is nearly isotropic, and is available at nighttime. Pixel geolocation in Level 1B data is obtained by intersecting the instant view axis of the imager instrument with the Earth reference ellipsoid, and thus the nominal image registration is accomplished assuming a zero elevation of observed scenes. Once these Level 1B data are reprojected from satellites pixel/line space to a geographical projection, any elevated scene exhibits a parallax displacement, which is different for images recorded at different viewing angles. With simple geometric transformations, the two parallax displacements from the two satellites can be directly related to the sought height. An algorithm developed at NASA Langley Research Center uses image subsets (chips) ranging from 8x8 to 20x20 pixel sizes to obtain a cross correlation between chips from the two image sources. Trying different relative displacements between the chips consecutively yields the highest correlation at the position of optimal displacement, which corresponds to the actual height for that image subset. Analyses indicate that we were able to achieve a subpixel accuracy when calculating the position of the highest correlation. This translates to a typical accuracy of the derived height on the order of 0.2-0.4 km. When the analyzed image chips have little texture, the correlation matching may fail for smaller chip sizes. In that case, a

larger chip can be used to obtain a reliable peak in the correlation profile, but that lowers the effective resolution of the resulting map of retrieved heights. More than 90% of image chips, however, were reliably matched using the 8x8 chip size, which helps to resolve smaller features and details within the eruption cloud, like the small peaks of cloud extending above 50 km altitude. Overall, we estimate the spatial resolution of the cloud top height retrieval product to be ∼4-6 km/pixel. This algorithm was applied to satellite data from 0400 to 2350 UTC on 15 January 2022 to quantify heights reached by the eruption cloud and document its temporal evolution.

Text S3.

To crudely estimate average propagation speed from Hunga to the receivers, we take advantage of the good visual correlation between the signals at balloon STR1 and stations IS22, IS07, IS36 and IS40 and cross-correlate time series of 3-minute 30-40 mHz-filtered signal variance between the reference station IS22 and the other records. The optimal lag Δt corresponding to maximum correlation is interpreted as caused by the difference in travel time between Hunga and the two sensors, i.e.:

$$\Delta t = \frac{d_s}{c_s} - \frac{d_{IS22}}{c_{IS22}} \tag{2}$$

where d_s is the sensor's range, d_{IS22} the range at IS22, c_{IS22} the average group velocity from Hunga to IS22, and c_s the average group velocity from Hunga to sensor. Without any prior knowledge of the event chronology or infrasound propagation speed, we cannot however anchor c_s which remains relative to c_{IS22}. To circumvent this issue, we assume that, range excluded, propagation properties are similar between IS22 and IS07. This is based on the premise that IS22 approximately lies on the orthodrome from Hunga to IS07

and that atmospheric conditions are relatively homogeneous along that path (see Fig. 1 a)), Note, however, that the lower boundary condition varies (from ocean to Australian land). Since we are interested in fitting the arrival times, or onsets, more than the position of the maxima, the lag-correlation is performed on decimal logarithm after setting values around the noise level of the sensor to zero. This manages sufficiently well to capture speed for short-range receivers, but fails where dispersion has important effect, such as at TTL4 with obvious double arrivals for WP1 and WP3. Hence, provided values are only indicative.

Finally, note that special care has to be taken with the balloons which are drifting during the day, affecting distance estimates. In order to account for that effect and since we are interested in average ground-relative propagation speeds, we first computed an approximate arrival time using a nominal propagation speed of 275 m/s. Then, the distance corresponding to the period of the arrivals was selected for a more precise estimate of distance and travel speed. Finally, reduced time

$$t_r = t - \frac{d(t)}{c_s} \tag{3}$$

used in Figure 4 is computed using the time-dependent range.

Text S4.

Figure S2 presents a comparison of background pressure power levels between ground station IS22 and balloon STR1 from January 16 00:00 UTC until 14:00 UTC (a period without any arrival from Hunga waves). This period includes some daytime at IS22 with increased noise levels due to turbulences and some nighttime with lower noise levels (see

Fig. 3 of the paper). Both average noise levels and 2nd and 98th quantile are shown to provide a sense of the different conditions encountered (weak vs large noise).

The background recorded on the balloons is clearly below what is observed on average at the ground (left panel), and mean balloon background only compares with the lowest values seen at IS22. This difference tends to increase towards higher frequencies. These statements concern raw pressure, but as we saw from PE calculations (Fig. 1 c)-e)) and the first overpasses (Fig. 4 b), scaled pressure is a more constant quantity and better suited for ground versus upper-air signal-to-noise ratio comparison in the Hunga case. Accounting for this effect and multiplying the balloon noise PSD by the scaling factor $\frac{\rho_{IS22}}{\rho_{STR1}}$, it becomes more comparable to that from ground receivers (right panel). In the infrasound range up to the 0.1 Hz (just below the microbarom peak at 0.2 Hz), weak noise conditions at the ground seem associated with a larger SNR at IS22 than in balloon data. However, both above that frequency and in strong noise conditions, there seems to be a significant advantage of upper-air measurements.

References

Podglajen, A., Hertzog, A., Plougonven, R., & Legras, B. (2016). Lagrangian temperature and vertical velocity fluctuations due to gravity waves in the lower stratosphere. *Geophysical Research Letters*, *43*(7), 3543–3553. doi: 10.1002/2016GL068148

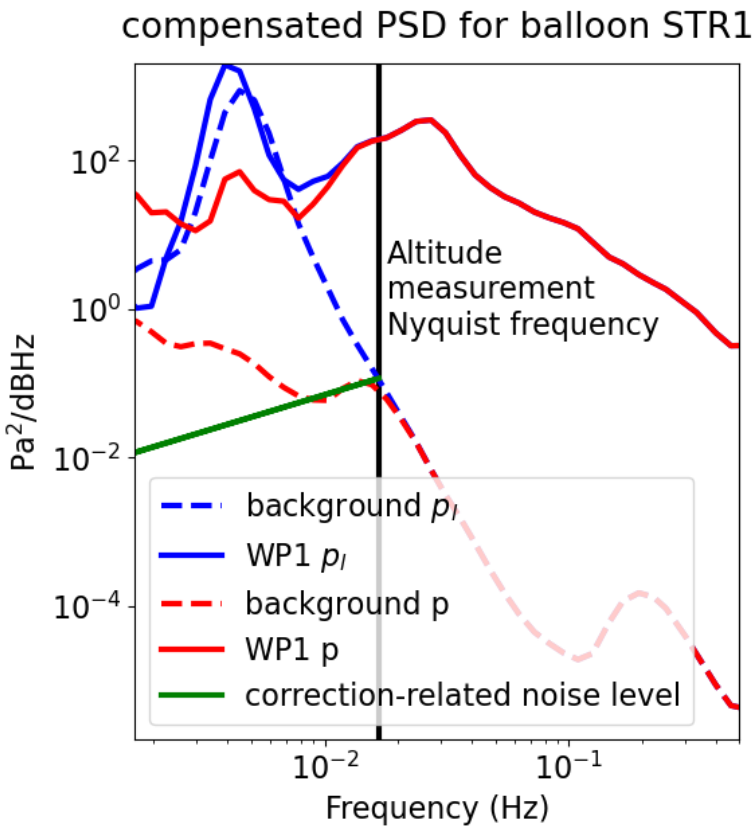

Figure S1. Compensated power spectral density of balloon STR1 raw pressure data p_l and pressure data p corrected for vertical oscillations using Eq. (1), during the overpass of WP1 and a background pre-eruption period. The impact of limited temporal resolution and precision of altitude measurements is illustrated by the black lines, which show the corresponding Nyquist frequency and estimated induced noise level.

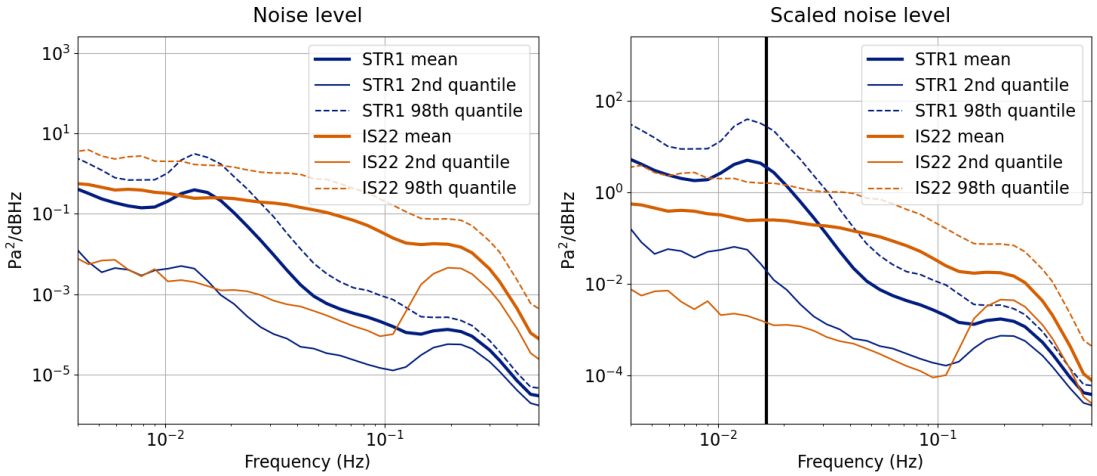

Figure S2. (Left) Compensated power spectral density of background pressure variability recorded ("noise") by IS22 and STR1 from Jan. 16 00:00 UTC to Jan. 16 14:00 UTC. (right panel) Same as left, but the balloon background signal is scaled by $\frac{\rho_s}{\rho_b}$, to mirror a signal-to-noise ratio by accounting for infrasound signal decrease (i.e. relative increase of noise) with decreasing ambient density.